Numerical Modeling of Corona Discharges in Asymmetric Electric Fields

Rakshit Tirumala

Institute Pprime
Departement Fluides, Thermique et Combustion
University of Poitiers, France
phone: (33) 06 15 90 10 23
e-mail: rakshit.tirumala.kumara@univ-poitiers.fr

David B. Go

Dept. of Aerospace and Mechanical Engineering
University of Notre Dame, USA
phone: (1) 574-631-8394
e-mail: dgo@nd.edu

***Abstract*— Numerical modeling of corona discharges has followed the same set of procedures for many years. The studies that simulate corona discharges on large scales for ionic wind generation or electrostatic precipitation often neglect the ionization events that occur near the source electrode and model only positive ion drift. The studies that model the ionization zone are often concerned with the species chemistry and consider a uniform axisymmetric configuration. However, with the increasing applications of corona discharges in millimeter and micron scales, the combination of the two procedures is necessary to accurately capture the discharge physics and ion distribution. The present study conducts numerical simulation of a wire-cylinder positive corona using both the purely ion-drift model and a model that includes species production and loss. A configuration where the wire is offset from the cylinder axis such that the electric field is asymmetric is considered. The study demonstrates the necessity of including the generation terms in the charge transport equations to obtain improved accuracy, particularly in gap dimensions comparable to the size of the ionization zone.**

I. INTRODUCTION

Corona discharges are partially ionized gas discharges that occur between a sharp electrode (called a corona source), typically a needle or a wire, and a blunt electrode (called a collecting electrode or counter electrode) such as a plate or a cylinder. A corona discharge can be operated in direct current (DC) mode and alternating current (AC) mode or in pulsed mode. DC corona discharges can be operated in both positive and negative po-

larity, depending on the whether the high voltage is applied to the corona source or the collecting electrode. Corona discharges have been a field of study since early in the 20th century as a detrimental mode of breakdown in high voltage conductors. Since then, corona discharges have been studied for various applications including electrostatic precipitation [1], flow generation and control [2], ion sources for mass spectrometers [3] and ozone generation [4]. Electrostatic precipitation and flow generation are particularly interesting applications as they both capitalize on the electrohydrodynamic (EHD) flow or ionic wind generated by the drift of ions away from the corona source to the counter electrode. In the 1990's, advancement in electronics renewed interest in corona discharges as an alternative technology for convective heat transfer, both as a mechanism for spot cooling [5] [6] and for the development of ionic wind blowers [7] [8] [9] [10]. In particular, corona discharges are governed by physical laws that are theoretically favorable to scaling [11], an advantage given the recent trend in miniaturization of devices.

While many researchers have studied corona discharges over the years both experimentally and numerically, the studies have been primarily experimental with numerical simulations used as a supplementary tool. This is frequently driven by the fact that corona discharge simulations are often not very predictive due to both the complex nature of the phenomena and the practical susceptibility of corona discharge experiments to experimental variability. Studies on numerical simulation of corona discharges are typically split into two camps, those that simulate the ionization zone alone and those that simulate the drift region alone. The former consists of groups primarily interested in studying the reaction chemistry within the ionization zone [12] [13] [14] [15] with the intention of mapping the concentrations of various species produced. The latter [16] [17] [18] [19] primarily focus on the drift of ions in the interstitial gap with the intention of studying its effects on EHD flow or interactions of the discharge with externally driven bulk flow. However, with the increased application of corona discharges and the resultant ionic wind in various fields, it becomes imperative to develop the numerical models to a level of accuracy required for their implementation as predictive design tools. Towards this end, it is necessary to bridge the gap between charge generation studies and charge transport studies in order to obtain accurate information regarding both the distribution of charged species as well as the generated ionic wind.

Recently, corona discharges have been studied in various configurations that induce a non-uniform electric field in the region of the corona source. These configurations include either asymmetric arrangements [7] [17] [20] of the two electrodes or the use of multiple electrodes, with either multiple corona electrodes [9] or multiple collecting electrodes [10] [21] or both. Predominantly, numerical simulations of corona discharges have been conducted under certain assumptions. The few studies that have modeled the reaction chemistry [12] [14] within the corona's ionization zone have done so in a one-dimensional field, thus analyzing a uniform (in this case, axisymmetric) electric field and charge density distribution in the region. The macroscopic procedure, that models only the ion transport within the discharge by solving coupled Poisson's and drift-diffusion equations [16] [17] [20], artificially injects a spatially uniform distribution of charge around the corona electrode and neglects the production of ions through electron-neutral interactions. In most studies, a uniform charge distribution is implemented irrespective of the variation of electric field in the proximity of the electrode surface. However, asymmetric electrode arrangements and multiple electrode configurations induce a non-

uniform distribution of electric field in the ionization region, particularly around the corona electrode. In such cases, the validity of the application of either of these procedures is not certain because the generation and distribution of charged species around the corona electrode is inherently coupled to the local magnitude of the electric field. While the existence of non-uniform electric fields is true even in simple configurations like point-to-plane coronas, because of the relatively large size of the gaps compared to the dimensions of the ionization zone, the drift model with uniform charge injection yields acceptable results in many of the past studies by various groups. However, in millimeter scale coronas, further analysis is required to ascertain the accuracy of this model.

In the present study, the authors analyze the differences between the two modeling procedures that include and discount ion production, with the intent of characterizing the validity of applying the purely ion-drift models to asymmetric configurations. A wire-cylinder configuration is considered for its simplicity and the corona is operated in positive polarity. The numerical results are compared with results from experiments to determine the relative accuracy with which the models predict the results. The work in this study extends the procedure of Chen and Davidson [12] to two dimensions and asymmetric electric field distribution.

II. CONFIGURATION AND EXPERIMENTAL SETUP

A wire-in-cylinder configuration was chosen because of its relative simplicity, both for grid generation as well as for specifying the boundary conditions. A schematic of the configuration is shown in Fig.1 along with the experimental setup. The collecting cylinder is 3 mm in radius, and wires of three radii (25 μm, 50 μm and 100 μm) were used as the corona source. A positive potential was applied to the wire and the cylinder was grounded. A non-uniform, asymmetric electric field was generated in the discharge region by moving the wire off-center by a distance δ. In the case where the wire was located off-center in an eccentric configuration, it was closer to the bottom half as shown in Fig. 1b. In concentric wire-cylinder discharges, as modeled in [12] [14], because of the axisymmetric nature, the value of the electric field at the wire's surface is uniform all around the wire. Because of the eccentric wire location in the present study, the electric field distribution varies along the wire's surface, which is referred to as a non-uniform or asymmetric electric field. Similar configurations have been used by other researches [17] [20] to study heat transfer augmentation in circular tubes using the Transport Model.

Experiments were conducted to obtain the voltage-current characteristics to compare with the models. In the experiments, the cylinder was bifurcated into two halves and separated by thin dielectric spacers so that current could be measured individually on the two halves (I_1 and I_2). Experiments were conducted with wires of diameter 50 μm and 100 μm, and a value of 1 mm for δ. A Bertan 225 high-voltage DC power supply was used as to apply voltage to the corona source and two Keithley 6485 picoammeters were used to measure the current through the two halves of the collecting electrode.

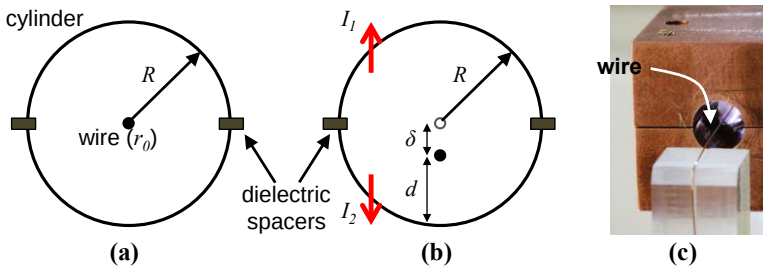

Fig. 1. Wire-in-cylinder configuration with (a) the wire concentric and (b) the wire eccentric by a distance δ. Dielectric spacers are used to separate the halves of the cylinder. I_1 and I_2 are the currents measured on each of the halves. (c) A picture of the experimental setup.

III. NUMERICAL MODELS AND PROCEDURE

A. Description of the Numerical Models

Fluid models of a corona discharge typically consist of solving Poisson's equation for the electric field, Eq. (1), and a set of scalar drift-diffusion equations, Eq. (2), for the charge transport

$$\nabla^2\Phi = -\nabla \bullet \overline{E} = -\frac{\rho}{\varepsilon_0}, \qquad (1)$$

$$\nabla \bullet \left(\rho_i \mu_i \overline{E} - D_i \nabla \rho_i\right) = S_i, \qquad (2)$$

where the subscript i reflects the charge species of interest; electrons (e), positive (p) and negative ions (n). Here, ρ_i is the charge density of species i, μ_i is the species mobility in air, and D_i is the species diffusivity in air. $\overline{E}$ is the electric field, Φ is the potential, ε_0 is the permittivity in free space, and ρ is the net space charge density ($\rho = \rho_p - \rho_e - \rho_n$). S_i accounts for the production or depletion of the charge species i and is typically dependent on the charge density of the other species involved in the discharge as well as the electric field. Hence, this is the term that couples the ionization and reaction chemistry of the various charge species. The product of mobility and electric field ($\mu_i \overline{E}$) gives the drift velocity of the charge species in the presence of an electric field. Diffusion is often neglected because its flux is a few orders of magnitude lower than the electric field driven drift flux. Two models will be compared in this section, both of which use the same basic equations described above.

The first model that is widely used to model positive corona discharges in macroscopic geometries will henceforth be called the Transport Model. This model, as the name implies, solves only the transport of ions through the interstitial space, neglecting any source terms. The size of the ionization zone is assumed to be negligible when compared to the gap distance between the electrodes and is hence neglected. As an extension of this assumption, the ion distribution is assumed to be uniformly distributed around the corona

source. Only positive ions are considered in the entire model, since, outside the ionization zone, the density of electrons and negative ions is negligible in comparison. Thus, neglecting diffusion, the Transport Model reduces Eq. (2) to

$$\nabla \bullet \left(\rho_p \mu_p \overline{E}\right) = 0\,, \qquad (3)$$

where ρ_p is the positive ion charge density and μ_p is the ion mobility. Equation 3 is solved in conjunction with Eq. (1) to simulate the discharge. The boundary conditions of Eq. (1) are fixed potentials (Dirichlet conditions) on the electrodes and zero fluxes on any dielectric or symmetric boundaries (Neumann conditions). Equation (3) requires one boundary for the space charge density ρ_p. This is applied as an injection boundary condition on the surface of the corona source electrode, specified as ρ_{p0}, which physically represents the magnitude of ion density at the boundary of the ionization zone.

The second model being studied we will refer to as the Ionization Model. This model includes the transport equations for both electrons and positive ions as well as production (source) terms for both of these species. Negative ions were also included in initial trial analyses but the rate of production of negative ions is two orders of magnitude lower than that of positive ions and hence their contribution to the current was negligible. For this model, Eq. (2) therefore reduces to

$$\nabla \bullet \left(\rho_e \mu_e \overline{E}\right) = -(\alpha - \beta)\left(\rho_e \mu_e |E|\right); \qquad (4a)$$

$$\nabla \bullet \left(\rho_p \mu_p \overline{E}\right) = +(\alpha)\left(\rho_e \mu_e |E|\right)\,. \qquad (4b)$$

In the two production terms, α is Townsend's first ionization coefficient, which quantifies the number of ionizing collisions between electrons and molecules per unit path length, and β is the similar coefficient for electron attachment (resulting in negative ion formation). Since an electron impact with a neutral molecule results in the production of a positive ion and an additional electron, the rate of production of both ions and electrons is coupled by the local charge concentration of electrons. α and β are non-linear functions of the local electric field and are modeled with the empirical equations [12]

$$\begin{aligned} \alpha &= 3.63\times10^5 \exp\left(-1.68\times10^7 / E\right)\ 1/m \quad \left(1.9\times10^5 < E < 4.56\times10^6\ \ V/m\right) \\ \alpha &= 7.36\times10^5 \exp\left(-2.01\times10^7 / E\right)\ 1/m \quad \left(4.56\times10^6 < E < 2\times10^7\ \ V/m\right) \end{aligned}; \qquad (5a)$$

$$\beta = 1.482\times10^3 \exp\left(-3.465\times10^6 / E\right)\ 1/m\,. \qquad (5b)$$

Near the wire surface, α is two orders of magnitude higher than β, but due to a more rapid decrease of α with reducing electric field, α and β become equal at a certain distance away from the wire surface [12] [22]. This location, where the electron production by ionization is balanced by its depletion through attachment marks the boundary of the

ionization zone. At atmospheric pressures, this equality occurs when the local electric field strength is the critical field strength, which for atmospheric air is ~3×10^6 V/m [12] [22] [23]. Note that negative ion formation is accounted for in Eq. (4a) and is used to define the ionization zone, even though negative ions are not modeled explicitly. Thus, Eq. (4a) and (4b) do not exactly conserve charge. However, given the negligible impact of negative ions on the overall current, reducing the number of equations did facilitate faster computation.

Equations (4a) and (4b) are both hyperbolic and require one boundary condition each, one for positive ions and one for electrons. In a positive corona discharge, the corona source is the anode and hence all positive ions move away from it. Hence a value of $\rho_p = 0$ is set on the source boundary. The electron charge density ρ_e then decides the total current generated by the discharge. Since the electron production is relatively small outside the ionization zone, a value of $\rho_e = \rho_{e0}$ is set for the entire gap beyond the boundary where $|E| = 3\times10^6$ V/m and ρ_e is solved for only within the ionization zone.

In both the Transport and Ionization Model, a Dirichlet boundary condition is required that ultimately dictates the current through the computational domain; ρ_{p0} on the corona source boundary for the former and ρ_{e0} on the ionization zone boundary for the latter. Often times, when the Transport Model is used, the value of ρ_{p0} is predicted *a priori* using a combination of Kaptzov's hypothesis [24] and Peek's breakdown criterion [23]. However, this approach has had limited success in predicting experimental currents. Further, it is unclear how to utilize Kaptzov's hypothesis when the field distribution around the corona source will clearly be non-uniform, as studied here. An alternative, semi-empirical approach is used where the value of ρ_{p0} in the Transport Model and ρ_{e0} in the Ionization Model, are specified in order to match a measured experimental current [18]. As with the Kaptzov's approach, this procedure also requires iteration as the current is modulated by the amount of space charge in domain when the model converges. This is the approach taken here.

B. Numerical Procedure

Since Eq. (2) is a first order hyperbolic equation, the method of characteristics was used to solve the charge transport equations for ρ_p and ρ_e. In Eq. (2), as well as in the case of the related Eqs. (3) and (4), the characteristics are simply the electric field lines. Taking advantage of the closed geometry, an elliptic grid was used to discretize the domain. The entire physical domain is split along the line of symmetry. Figure (2) shows the discretized domain. Orthogonality at the wire and cylinder boundaries (Fig. (2) inset) was implemented using the procedure in Thompson et al. [25]. The elliptic grid reduces both the Poisson's equation and the charge transport equation to equivalently one dimensional equations along the respective field lines.

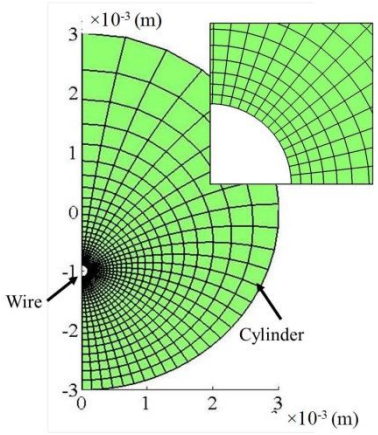

Fig. 2. The simulation domain with a generated grid of 30×30 points. Inset shows the orthogonality at the surface of the wire.

IV. RESULTS AND DISCUSSION

To compare the Transport and Ionization Models and to check their validity, the parameter $I_{ratio} = I_1/I_2$ was evaluated and compared with the experimental data for the eccentric configuration case with (δ = 1 mm). This parameter represents the percentage of current that flows through the portion of the cylinder farther from the corona source rather than the portion closer to the corona source, and therefore provides an indication of the distribution of ions around the discharge volume. When the corona source is centered, this ratio is $I_{ratio} = 1$ because of symmetry, and both Models along with experiments confirmed this. In the eccentric cases, we anticipate the $I_{ratio} < 1$ as more current with pass through the portion of the cylinder closer to the corona source.

Figure 3 plots the variation of I_{ratio} with the applied potential (Φ_0) for the two chosen wires of radii 50 µm and 100 µm. Data obtained from the two numerical models are presented along with experimental results. As can be seen from the figures, the values predicted by the Ionization Model are a significantly better match to the experimental data.

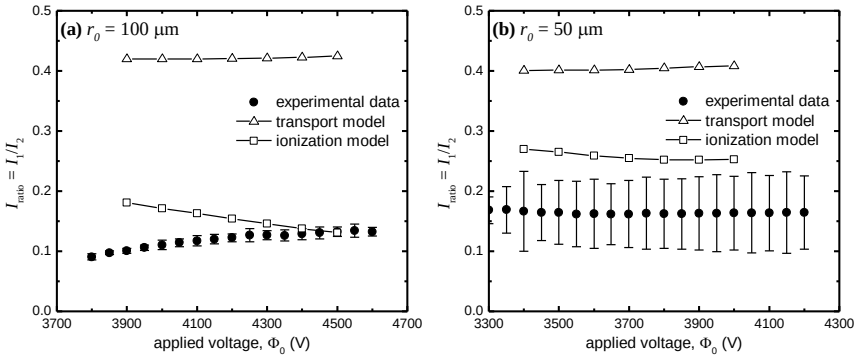

Fig. 3. The variation of I_{ratio} with the applied voltage (Φ_0) for (a) wire with r_0 = 100 μm and (b) wire with r_0 = 50 μm. The error bars represent the precision uncertainty from multiple experimental trials at 95% confidence.

As shown in Table 1, the computationally calculated I_{ratio} for r_0 = 100 μm (average = 0.16) matches well with the experimental value (average = 0.12). For r_0 = 50 μm however, the predicted value (average = 0.26) is relatively higher than the experimental value (average = 0.16). The prediction by the Transport Model (average ~ 0.4) is much higher for both the wire radii and predicts a far greater current to the further portion of the cylinder than measured experimentally.

TABLE 1: EXPERIMENTAL AND NUMERICAL VALUES OF I_{ratio} vs APPLIED VOLTAGE (Φ_0) FOR THE WIRES WITH (a) RADIUS 100 μm AND (b) RADIUS 50 μm.

(a) r_0 = 100 μm			
Voltage Φ_0 (V)	**Experiment**	**Ionization Model**	**Transport Model**
3900	0.10	0.18	0.42
4000	0.11	0.17	0.42
4100	0.12	0.17	0.42
4200	0.12	0.16	0.42
4300	0.13	0.15	0.42
4400	0.13	0.15	0.42
4500	0.13	0.14	0.42
Average	0.12	0.16	0.42

(b) r_0 = 50 μm			
Voltage Φ_0 (V)	**Experiment**	**Ionization Model**	**Transport Model**
3400	0.17	0.27	0.40
3500	0.16	0.27	0.40
3600	0.16	0.26	0.40
3699	0.16	0.26	0.40
3800	0.16	0.25	0.41
3900	0.16	0.25	0.41
4000	0.16	0.25	0.41
Average	0.16	0.26	0.40

The primary reason for the better fit from the Ionization Model is the inclusion of ionization. In the Transport Model, the distribution of space charge in the discharge gap and, as a consequence, the variation of current density around the cylinder is dictated only by the asymmetry in the electric field. The uniform ion density distribution around the wire as applied by the boundary condition ρ_{p0} is simply redistributed in the gap by the asymmetric electric field. However, this does not account for the fact that charge creation is field dependent and thus should also be asymmetrically distributed. The Ionization Model, on the other hand, considers both asymmetric transport *and* asymmetric production of ions. The combination of the two results in a larger fraction of the current going to the closer collecting electrode. Figure 4 plots the positive ion charge density distribution from the two models for the same total current. As can be seen, there is a much higher angular distribution from the Ionization Model than in the Transport Model.

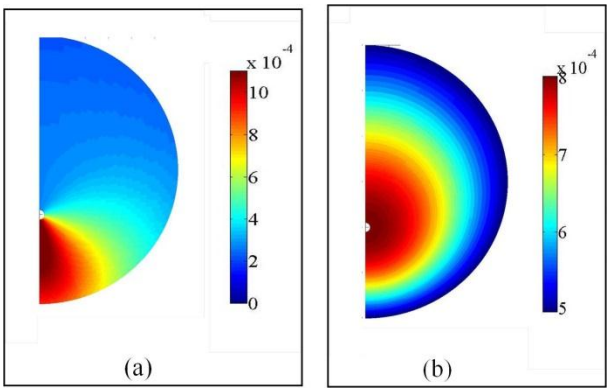

Fig. 4. Distribution of the positive ion density in (a) the Ionization Model and (b) the Transport Model for r_0 = 100 μm, R = 3 mm, δ = 1 mm, and Φ_0 = 4300 V. Note that the range of charge density values for the two plots are different.

Another way to assess this non-uniformity is to consider the current as a function of the angle along the wire surface θ. Figure 5 plots the variation of the normalized current density around the wire, $J_{wire}(\theta)/J_{wire}(\theta = 0)$, for both the Ionization Model and the Transport Model for three wire radii – 25 μm, 50 μm and 100 μm. It can be observed that the variation is much higher for the Ionization Model (solid lines) than for the Transport Model (dashed lines). Also, the relative variation among the Ionization Model data reduces as the wire radius decreases, slowly approaching the values of the Transport Model, which are almost uniform around the wire surface.

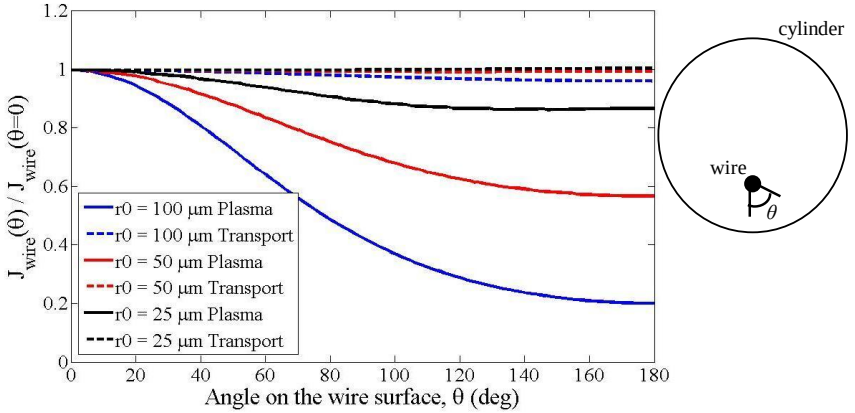

Fig. 5. Plot showing the variation of the normalized current density $J_{wire}(\theta)/J_{wire}(\theta = 0)$, around the wire surface for the Ionization Model (solid lines) and the transport model (dashed lines). Angle on the wire surface (θ) is defined as shown on the right. The applied voltages were Φ_0 = 4300 V, 3800 V, and 3100 V for r_0 = 100 μm, 50 μm, and 25 μm, respectively. For all cases R = 3 mm and δ = 1 mm.

Figure 6 plots the variation of the positive ion density (ρ_p) and the ionization coefficient (α) around the wire for the three wire radii for data from the Ionization Model. As can be seen from Fig. 6a, the positive ion density is not uniform around the wire surface as presumed by the Transport Model. These figures, in which the variations tend to even out for smaller wire radii, also demonstrate the decreasing effectiveness of the Ionization Model for wires with extremely small radii, where the values predicted by the two numerical models are similar and differ from the experiments significantly. Data on ionization and attachment coefficients, as well as on electron mobilities are sparse for electric fields > 2×10^7 V/m, a range which is achieved by the wires of radii 25 μm and 50 μm and the formulations used in this study may not be accurate. This could potentially be one reason to explain the discrepancies between the Ionization Model and the experimental data.

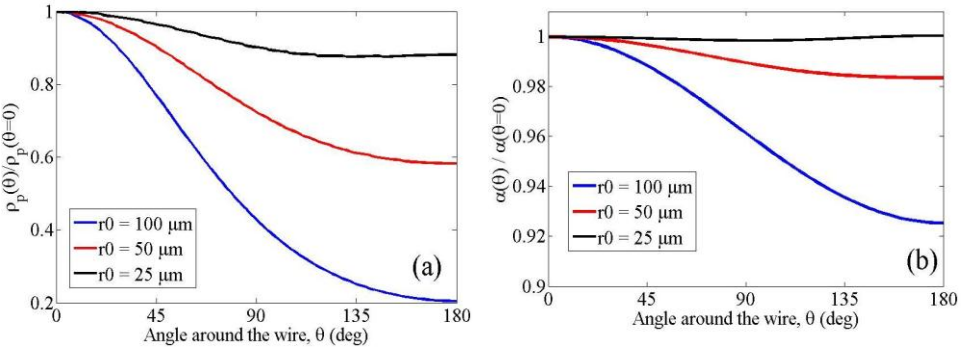

Fig. 6. Variation around the wire's surface of (a) positive ion density (ρ_p) and (b) ionization coefficient (α). The applied voltages were Φ_0 = 4300 V, 3800 V, and 3100 V for r_0 = 100 μm, 50 μm, and 25 μm, respectively. For all cases R = 3 mm and δ = 1 mm.

As the wire radius decreases, the electric field at the surface of the wire increases and the radius of the ionization zone decreases. Since the Ionization Model relies on the combined effects of asymmetry in electric field and in ionization, its predictions differ from the Transport Model only as long as the ionization zone is non-negligible. Since the size of ionization zone is related to the wire radius, the parameter d/r_0, where d is the shortest gap distance, represents the fraction of the interstitial space occupied by the ion-zone and can be employed to understand the behavior. To check this relation, the Ionization Model and Transport Model were repeated in two other conditions with cylinder radii (R) of 1.5 mm and 2 mm, and offset distances (δ) of 0.5 mm and 1 mm, such that the gap distances, d, was 1 mm in both cases. Table 2 shows the predicted ratios for the two models. For the same wire radius of r_0 = 25 µm, the difference between the Ionization Model and the Transport Model is more noticeable when d/r_0 is 40, rather than 80 as in the previous case. Eccentricity can be parameterized by the ratio R/δ, and it can be observed from Table 2 that the ratio of currents predicted by the Transport Model is dependent on this value. Experiments weren't conducted for the second and third set of geometric parameters (R = 1.5 mm and 2 mm), the intention only being to highlight the difference between the two models.

TABLE 2: VARIATION OF THE CURRENT RATIO (I_{ratio}) WITH THE ION-ZONE FRACTION PARAMETER (d/r_0) AND THE ECCENTRICITY PARAMETER (R/δ) FOR THE TWO NUMERICAL MODELS.

	r_0 [µm]	R [mm]	δ [mm]	d [mm]	d/r_0	R/δ	I_{ratio} Ionization Model	I_{ratio} Transport Model
Set-1	25	3.0	1.0	2.0	80	3	0.40	0.41
	50	3.0	1.0	2.0	40	3	0.27	0.41
	100	3.0	1.0	2.0	20	3	0.15	0.42
Set-2	25	1.5	0.5	1.0	40	3	0.27	0.42
	50	1.5	0.5	1.0	20	3	0.14	0.42
Set-3	25	2.0	1.0	1.0	40	2	0.16	0.24
	50	2.0	1.0	1.0	20	2	0.07	0.24

V. CONCLUSION

The study extends past numerical models to two dimensions and conducts simulations of corona discharges in asymmetric electric fields. The Ionization Model works reliably on both the small scales, predicting the events within the ionization zone, as well as on the macroscopic scales of predicting trends in current distributions. While the Transport Model is sufficient when the gap distances are far larger than the size of the ionization zone, the Ionization Model needs to be used when the zone is no longer negligible. The procedure can be extended to ionic wind generation by coupling the calculated space charge density with Navier-Stokes equations. The Ionization Model requires solving two

transport equations instead of one, but the similarity in the equations implies that it requires no extra effort procedurally. However, the Ionization Model requires significantly higher resolution at the wire surface, which is computationally more expensive. In addition, the Ionization Model allows for the inclusion of reaction chemistry in the design process, with an individual transport equation for each species, which can be used to predict ozone generation from ionic wind blowers.

ACKNOWLEDGEMENTS

The authors would like to acknowledge funding support from Intel Corporation.

REFERENCES

[1] H.R. Velkoff, I. Yamamoto, "Electrohydrodynamics in an electrostatic precipitator," *J. Fluid Mech.*, vol. 108, pp. 1-18, 1981.

[2] G. Artana, D. J, L. Leger, E. Moreau and G. Touchard, "Flow control with electrohydrodyamic actuators," *AIAA Journal*, vol. 40, no. 9, pp. 1773-1779, 2002.

[3] D.I. Carroll, I. Dzidic, R.N. Stillwell, K.D. Haegle, E.C. Horning, "Atmospheric pressure ionization mass spectrometry: corona discharge ion source for use in a liquid chromatography- mass spectrometry-computer analytical system," *Anal. Chem.*, vol. 47, pp. 2367-2373, 1975.

[4] C. Monge, R. Peyrous, B. Held, "Optimization of a corona wire-to-cylinder ozone generator: Comparison with economical criteria," *Ozone: Science and Engineering*, vol. 19, pp. 533-547, 1997.

[5] F. Yang, N.E. Jewell-Larsen, D.L. Brown, K. Pendergrass, D.A. Parker, I.A. Krichtafovitch, A.V. Mamishev, "Corona driven air propulsion for cooling of electronics," in *XIII Int'l. Sympos. High Voltage Engineering (ISH)*, Rotterdam, The Netherlands, 2003.

[6] D.B. Go, S.V. Garimella, T.S. Fisher, R.K. Mongia, "Ionic winds for locally enhanced cooling," *J. Appl. Phys.*, vol. 102, p. 053302, 2007.

[7] N.E. Jewell-Larsen, E. Tran, I.A. Krichtafovitch, A.V. Mamishev, "Design and optimization of electrostatic fluid accelerators," *IEEE Trans. Dielectr. Electr. Insul.*, vol. 13, pp. 191-203, 2006.

[8] J.S.Chang, H. Tsubone, G.D. Harvel, K. Urashima, "Narrow flow channel driven EHD gas pump for an advanced thermal management of microelectronics," *IEEE Trans. Ind. App.*, vol. 46, pp. 1151-1158, 2010.

[9] J. Zhang, F.C. Lai, "Effect of emitting electrode number on the performance of EHD gas pump in a rectangular channel," in *Annual Meeting Electrostatics Society of America*, Charlotte, USA, 2010.

[10] R. Tirumala, D. B. Go, "Multi-electrode assisted corona discharge for electrohydrodynamic flow generation in narrow channels," *IEEE Trans. Dielectr. Electr. Insul.*, vol. 18, no. 6, pp. 1854-1863, 2011.

[11] R. Tirumala, Y. Li, D. A. Pohlman and D. Go, "Corona discharges in sub-millimeter electrode gaps," *J. Electrostatics*, vol. 69, pp. 36-42, 2011.

[12] J. Chen, J.H. Davidson, "Electron density and energy distributions in the positive DC corona: Interpretation for corona-enhanced chemical reactions," *Plasma Chemistry and Plasma Processing,* vol. 22, pp. 199-224, 2002.

[13] J. Chen, J.H. Davidson, "Ozone production in the positive DC corona discharge: Model and comparison to experiments," *Plasma Chemistry and Plasma Processing,* vol. 22, pp. 495-522, 2002.

[14] K. Yanallah, F. Pontiga, A. Fernandez-Rueda, A. Castellanos, "Experimental investigation and numerical modelling of positive corona discharge: ozone generation," *J. Phys. D: Appl. Phys.,* vol. 42, p. 065202, 2009.

[15] K. Yanallah, S. Hadj Ziane, A. Belasri, Y. Meslem, "Numerical modeling of ozone production in direct current corona discharge," *J. Molecular Structure,* vol. 777, pp. 125-129, 2006.

[16] N. E. Jewell-Larsen, P. Q. Zhang, C. P Hsu, I. A. Krichtafovitch, A. V.Mamishev, "Coupled-physics modeling of electrostatic fluid accelerators for forced convection cooling," in *9th AIAA/ASME Joint Thermophysics and Heat Transfer Conference*, San Francisco, CA, 2006.

[17] R. Lakeh, M. Molki, "Targeted heat transfer augmentation in circular tubes using a corona jet," *Journal of Electrostatics,* vol. 40, pp. 31-42, 2012.

[18] D.B. Go, R.A. Maturana, T.S. Fisher, S.V. Garimella, "Enhancement of external forced convection by ionic wind," *Int'l. J. Heat Mass Transf.,* vol. 5, pp. 6047-6053, 2008.

[19] P. Atten, K. Adamiak, "Simulation of corona discharge in point-plane configuration," *J. Electrostatics,* vol. 61, pp. 85-98, 2004.

[20] R. Lakeh, M. Molki, "Patterns of Airflow in CircularTubes Caused by a Corona Jet With Concentric and Eccentric Wire Electrodes," *Journal of Fluids Engineering,* vol. 132, no. 1, p. 081201, 2010.

[21] K. Adamiak, X. Deng, "The electric corona discharge in a triode system," *IEEE Trans. Ind. Appl.,* vol. 35, pp. 767-773, 1999.

[22] R. Morrow, J.J.Lowke, "Streamer propagation in air," *J. Phys. D: Appl. Phys.* , vol. 30 , no. 4, pp. 614-627, 1997 .

[23] J. F.W. Peek, Dielectric phenomenon in high voltage engineering, McGraw-Hill Book Company, 1915.

[24] N. Kaptzov, Elektricheskiye yavleniya v gazakh i vacuume, OGIZ, 1947.

[25] F. Thompson, B.Soni, N. Weatherill, Handbook of Grid Generation, New York: CRC Press, 1999.